Downloaded from SAE International by Frank Tittel, Wednesday, June 27, 2018

SAE TECHNICAL PAPER SERIES

2004-01-2266

Development of Optical Trace Gas Monitoring Technology for NASA Human Space Flight

J. Houston Miller, Andrew R. Awtry and Brendan McAndrew
The George Washington University

Frank K. Tittel and Anatoliy A. Kosterev
Rice University

Rui Q. Yang, Cory J. Hill, Chung M. Wong, Baohua Yang and Greg Bearman
The Jet Propulsion Laboratory

34th International Conference on Environmental Systems (ICES)
Colorado Springs, Colorado
July 19-22, 2004

SAE International™

400 Commonwealth Drive, Warrendale, PA 15096-0001 U.S.A. Tel: (724) 776-4841 Fax: (724) 776-5760 Web: www.sae.org

Downloaded from SAE International by Frank Tittel, Wednesday, June 27, 2018

All rights reserved. No part of this publication may be reproduced, stored in a retrieval system, or transmitted, in any form or by any means, electronic, mechanical, photocopying, recording, or otherwise, without the prior written permission of SAE.

For permission and licensing requests contact:

SAE Permissions
400 Commonwealth Drive
Warrendale, PA 15096-0001-USA
Email: permissions@sae.org
Fax: 724-772-4891
Tel: 724-772-4028

For multiple print copies contact:

SAE Customer Service
Tel: 877-606-7323 (inside USA and Canada)
Tel: 724-776-4970 (outside USA)
Fax: 724-776-1615
Email: CustomerService@sae.org

ISSN 0148-7191
Copyright © 2004 SAE International

Positions and opinions advanced in this paper are those of the author(s) and not necessarily those of SAE. The author is solely responsible for the content of the paper. A process is available by which discussions will be printed with the paper if it is published in SAE Transactions.

Persons wishing to submit papers to be considered for presentation or publication by SAE should send the manuscript or a 300 word abstract of a proposed manuscript to: Secretary, Engineering Meetings Board, SAE.

Printed in USA

Downloaded from SAE International by Frank Tittel, Wednesday, June 27, 2018

2004-01-2266

Development of Optical Trace Gas Monitoring Technology for NASA Human Space Flight

J. Houston Miller[†], Andrew R. Awtry[†], Brendan McAndrew[†], Frank K. Tittel[‡] , Anatoliy A. Kosterev[‡], Rui Q. Yang[▪] , Cory J. Hill[▪], Chung M. Wong[▪], Baohua Yang[▪], and Greg Bearman[▪]
[†] The George Washington University, [‡]Rice University,
[▪] The Jet Propulsion Laboratory

Copyright © 2004 SAE International

ABSTRACT

Investigators from three institutions have partnered in a Rapid Technology Development Team whose goal will be the deployment of laser-based sensors for air-constituent measurements on board spacecrafts. The sensors will eventually be based on Type II Interband Cascade (IC) lasers being developed at the Jet Propulsion Laboratory. These lasers will be used in implementations of both photo acoustic spectroscopy based on the use of quartz tuning fork oscillators as a resonant acoustic sensor (QE-PAS) and cavity ring down spectroscopy (CRDS). In the first year of the program, work at Rice and George Washington Universities has focused on the development of both QEPAS and CRDS sensors for ammonia using near infrared lasers. Simultaneously, the JPL portion of the team has fabricated both Fabry Perot and distributed feedback lasers in the mid infrared that can be used for formaldehyde detection. Features of both sensing technologies as well as the benefits of measurements at longer wavelengths will be presented.

INTRODUCTION

Manned space missions planned for the next century will include longer stays aboard the International Space Station, expeditions to Mars, as well as return trips to the moon. Although widely different in specific mission objectives, extended stays in space share a common need to create and maintain an environment suitable for human habitation. Durations on the order of months, or years, will require recycling of both air and water. Technologies must be in place to monitor the performance of reprocessing systems, and to reduce the risk of high-integrated exposures. This paper introduces a collaborative research project whose goal is to create trace gas monitors based on optical sensing for NASA human space flight use.

Optical sensing technologies

An understanding of all optical absorption strategies usually begin with some variation of the extinction equation:

$$I = I_o \cdot e^{-\alpha \cdot l} \tag{1}$$

where α is the extinction coefficient, I_0 is the radiation intensity incident on a sample, and I is the sample intensity at the detector. In the case of the molecular absorption from a single rotational line in a vibrational band, the extinction coefficient is given by:

$$\alpha = S \cdot g \cdot \rho \cdot x_j \tag{2}$$

here S is the line strength, g is the line shape factor, ρ is the molecular density, and x_j is the mole fraction (or mixing ratio) of the target species.

In this program, we wish to address sensing for a variety of target species at first using commercially available laser sources in the near infrared and later in the program shifting our work to mid-infrared wavelengths. The goal of every absorption technique is to make as sensitive a measurement of α as possible. In using semiconductor lasers as the excitation source, a variety of techniques have been developed over the past two decades including direct absorption (comparing signal levels at a detector downstream of a sample on and off resonance), low frequency modulation (also known as wavelength modulation spectroscopy), high

Downloaded from SAE International by Frank Tittel, Wednesday, June 27, 2018

frequency modulation, photoacoustic detection, and cavity ring down spectroscopy. Each technique has characteristic advantages and disadvantages that usually lead to a compromise between instrument complexity and sensitivity.

In the next few pages we will introduce the conceptual framework for both cavity ring down and photoacoustic spectroscopies and describe their technical implementation of each at Rice and George Washington Universities. Both techniques have been applied to ammonia detection in the near infrared using commercial diode lasers. Next, progress in the development of mid-infrared lasers at the Jet Propulsion Laboratory will be described. Finally, potential detection limits for the detection of formaldehyde (H_2CO) using this system will be projected.

MAIN SECTION

QUARTZ-ENHANCED PHOTOACOUSTIC SPECTROSCOPY

In photoacoustic spectroscopy, energy absorbed by molecules is converted into thermal energy, and an expansion of the heated volume occurs. Hence, a modulated laser beam at the appropriate optical frequency results in a sound wave in the medium, which can be detected by a sensitive microphone. The amount of absorbed power is proportional to the concentration of the absorbing species, and therefore the intensity of the acoustic wave can be used for concentration measurements. The photoacoustic signal is proportional to the absorption coefficient, the laser power, and inversely proportional to the modulation frequency *f*. A common approach to increase the detection sensitivity when compact low-power CW laser sources are used is to utilize an acoustic resonator with a quality factor *Q*, typically ~50 [2-4]. The laser power or wavelength is then modulated at the resonant acoustic frequency (or half the resonant frequency, if 2*f* detection is used), usually 1,000 – 5,000 Hz. If this approach is used, the absorbed laser power is accumulated in the acoustic mode of the resonator during Q oscillation periods. Therefore, in this detection mode the acoustic signal is proportional to the effective integration time $t=Q/f$.

Traditional PAS suffers from background acoustic noise and sampled gas flow noise. The Rice group has implemented a novel version of PAS in which the "microphone" is an inexpensive quartz tuning fork oscillator operating at 32,768 (i.e. 2^{15}) Hz with a Q of ~10,000 in ambient air [3, 5]. In order to enhance the photoacoustic pressure, an acoustic microresonator is added. The microresonator consists of two glass tubes, each 2.45 mm long with a 0.32mm inner diameter, aligned with the laser beam perpendicular to the TF plane. The laser wavelength is modulated at $f_0/2$ frequency with an amplitude sufficient to cover the target absorption line. The piezoelectric current generated by the TF is converted to voltage by means of a transimpedance preamplifier and subsequently rectified at f_0 frequency in a lock-in amplifier. The gas cell used in this work is depicted in Figure 1. It was fabricated from a standard NW25 vacuum flange and equipped with two sapphire windows, two gas throughputs, and a piezoresistive pressure transducer. The estimated cell volume is ~1cm^3.

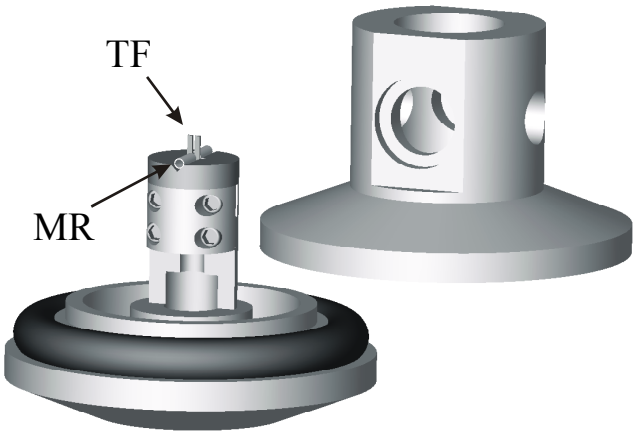

Figure 1 .Sketch of the QEPAS gas cell. MR-microresonator, TF-quartz tuning fork. All parts are drawn to scale except for the MR whose actual size is smaller and its position is closer to the TF opening. The top opening in the enclosing flange is for a pressure transducer, right and left openings are for the gas input and output, and front and back are for optical windows.

For both QEPAS and CRDS (described below) the absorption line selection for NH_3 detection was based on data published in [1]. A line at 6528.76 cm^{-1} was chosen as a target. At pressures greater than 500 torr this line is merged with its weaker neighbor at 6528.89 cm^{-1}. Simulated absorption spectra are shown in Figure 2(a). A fiber-coupled DFB telecommunication diode laser (NTT Electronics Corporation model NLK1C5J1AA) was used as a spectroscopic source. The laser power delivered to the TF at the target wavelength was measured to be 38 mW. A permeation tube based gas standards generator (Kin-Tek model 491 M) was used to generate calibrated trace concentrations of NH_3 in ultra high purity (UHP) N_2. All the measurements were performed using a steady state gas flow to reduce adsorption-desorption effects, typically 50 sccm (cubic centimeters per minute referred to standard temperature and pressure) N_2 mass-flow. Sample QEPAS spectra of 50 ppmv NH_3:N_2 are shown in Figure 2(b).

The amplitude of the detected QEPAS signal is determined by the following factors:

1. Peak intensity of the absorption line,
2. V-T energy transfer rate of the molecule,
3. The TF Q-factor,
4. An enhancement factor of the microresonator,
5. Laser modulation depth.

Downloaded from SAE International by Frank Tittel, Wednesday, June 27, 2018

Factors 1-4 are pressure dependent, and 5 has to be optimized to match the pressure-dependent absorption line width. We mapped QEPAS signal corresponding to the peak absorption as a function of gas pressure and laser current modulation depth (Figure 3). The measurements were carried out with a 50 ppmv NH_3 in N_2 mixture as described above. It is evident that the highest signal is observed at 60 Torr. The signal amplitude decreases at higher pressures until the absorption lines start to merge at 500 Torr. The atmospheric pressure (764 Torr) signal is ~10% weaker than the signal at 500 Torr.

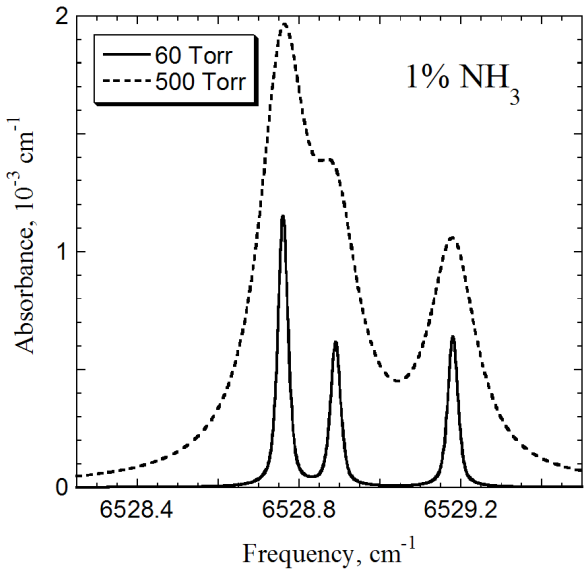

Figure 2: (a) Simulated ammonia absorption based on spectroscopic parameters from Ref. [1]. (b) QEPAS spectra of the same lines acquired at 50 ppmv NH_3 concentration and a 0.3 s lock-in amplifier time constant.

The sensitivity is determined by the SNR, and it was verified in several experimental tests that the observed QEPAS noise is equal to the theoretical thermal noise of the TF at its resonance frequency [6].

$$\frac{\sqrt{\langle V_N^2 \rangle}}{\sqrt{\Delta f}} = R_{fb}\sqrt{\frac{4k_B T}{R}} \qquad (3)$$

$$R = \frac{1}{Q}\sqrt{\frac{L}{C}} \qquad (4)$$

where $\sqrt{\langle V_N^2 \rangle}$ is the RMS voltage noise observed at the transimpedance amplifier output, Δf is the detection bandwidth, R_{fb} is the amplifier feedback resistor, T is the TF temperature, R, L, and C are the electrical parameters of the TF when it is represented by the equivalent serial resonant circuit. From Eq. 3 and 4, it follows that the noise is inversely proportional to the $\sqrt{Q}$, and the Q-factor changes from 31 000 at 30 Torr to 12 600 at 500 Torr. The sensitivity at atmospheric pressure is almost the same as at 60 Torr because the absorption lines merge.

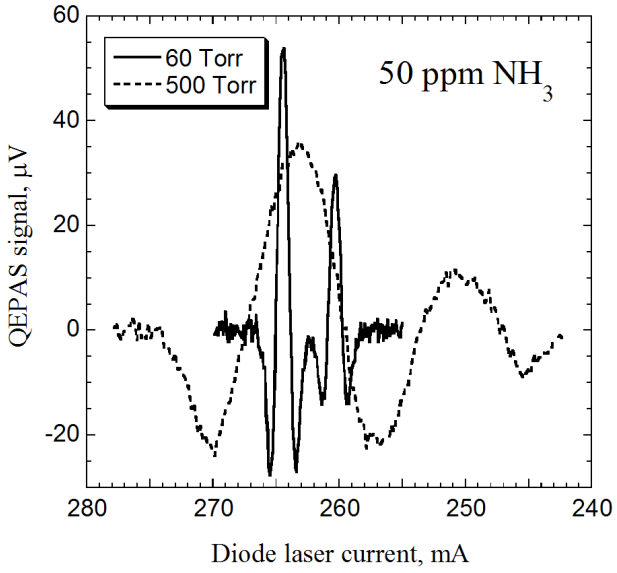

Figure 3: QEPAS signal at the transimpedance preamplifier output corresponding to the peak NH_3 absorption near 6528.8 cm^{-1} for different gas pressures and laser current modulation depth. All the measurements were performed at 50 ppmv NH_3 in N_2 and a 40 sccm gas mass flow.

The linearity and sensitivity of the sensor were verified by measuring its response to the changing NH_3 concentration in N_2 flow of 40 sccm. The measurements were performed at 60 Torr pressure in the TF cell, and the laser wavelength was locked to the center of the 6528.76 cm^{-1} NH_3 absorption line [1]. The results of repetitive measurements made every 1.5 s are plotted in Figure 4. The scatter of consecutive measurements at a certain concentration level also did not depend on the concentration and was in agreement with Eq. 3. Based on these data, the NH_3 concentration that would result in noise-equivalent (1σ) sensor readings is 0.65 ppmv, assuming a 1 s lock-in amplifier time constant, 50 Torr gas pressure and 38 mW optical excitation power. The corresponding absorption coefficient normalized to optical power and detection bandwidth is k=7.2×10^{-9} $cm^{-1}W/Hz^{½}$. This normalized sensitivity is only 4-5 times lower than the best results reported for conventional wavelength-modulation PAS [7] and somewhat better than reported for amplitude-modulation PAS [8].

In conclusion, it is demonstrated that the QEPAS approach can be used for trace gas detection with

Downloaded from SAE International by Frank Tittel, Wednesday, June 27, 2018

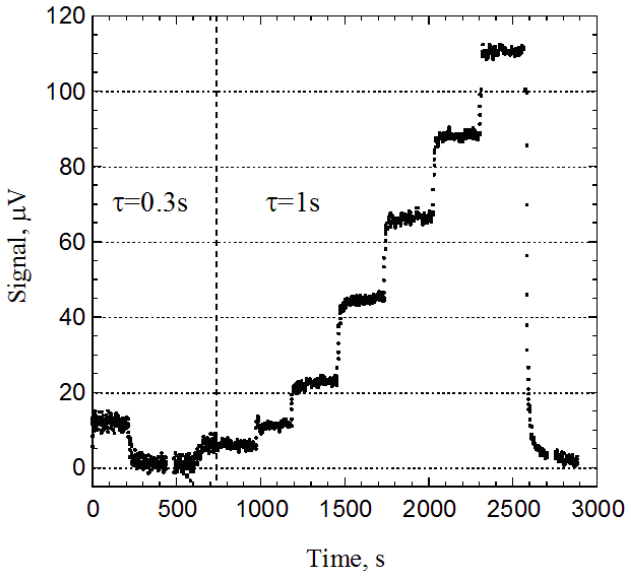

Figure 4: QEPAS signal (transimpedance preamplifier output) repetitively recorded while the NH_3 concentration was varied by changing the carrier gas flow in the gas standards generator.

commercially available near-IR lasers. The QEPAS sensitivity is in the same range as the sensitivity of conventional PAS with the added advantages of noise immunity and an ultrasmall sample volume. Ammonia concentrations resulting in noise-equivalent (1σ) sensor response is measured to be 0.65 ppmv (1s time constant), which corresponds to 3 ppbv if the laser at 10.1 μm would be used as an excitation sourse. Considerable gain in performance is expected if custom or modified TFs with lower resonant frequency would be used, because the photoacoustic signal is inversely proportional to the modulation frequency. The technology may also benefit from a better design and tighter tolerances of the acoustic microresonator.

CAVITY RING DOWN SPECTROSCOPY

Cavity ringdown spectroscopy (CRDS) is a sensitive absorption technique that is capable of monitoring a wide range of species. In *cw*-CRDS, a beam from a laser is injected into an optical cavity formed between two highly reflective mirrors. Only light with a frequency that matches a cavity transmission mode is coupled into the cavity due to constructive interferences. The energy of light at these resonant frequencies builds up in the cavity over time. When the energy reaches a set threshold, the input beam is shut off and a ringdown (the exponential loss of light from the cavity) is recorded [9-15]. The time constant for decay from the cavity, τ, can be related to concentration through:

$$\frac{1}{\tau} = \frac{1}{\tau_C} + c \cdot \alpha = \frac{1}{\tau_C} + c \cdot S \cdot g \cdot \rho \cdot x_j \qquad (5)$$

where τ_C is the time constant for decay from the empty cavity and c is the velocity of light. In the GWU laboratory, extinction coefficients of 3×10^{-9} cm^{-1} have been detected (as given by 3 times the standard deviation in the off-resonance background).

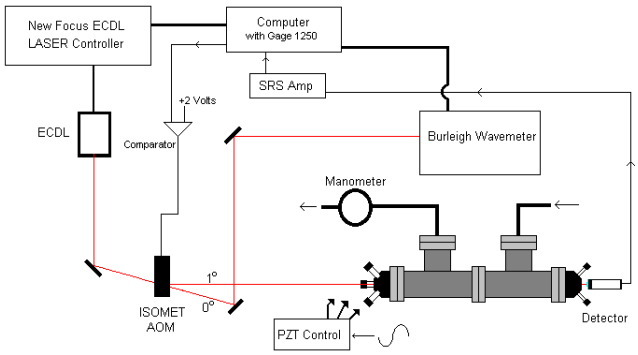

Figure 5: Schematic of CRDS experiment. ECDL stands for external cavity diode laser. AOM is an acousto-optic modulator

Experimental Details

The schematic layout of our *cw*-CRDS spectrometer is shown in Figure 5. The light source used was an external cavity diode laser manufactured by New Focus (Velocity 6328). The ECDL has a continuous wavelength range from 1510-1580 nm with a maximum power of 8mW (typical 6mW) and a bandwidth of 5 MHz. Tuning the laser is accomplished by changing the angle between the tuning mirror and the grating (in the laser housing). A DC motor is used to coarse tune, while a PZT attached to the mirror is used to fine-tune the laser.

A Burleigh wavemeter (WA-1000) was used to determine the wavelength of light emitted by the laser prior to the experiments. Calibration curves were then constructed which allowed for the determination of the wavelength for a given temperature and current for DFB lasers.

Over the last several years, our experimental protocol relied on a laboratory computer equipped with a Gage Compuscope 1250 digitzer card and a Keithley digital-to-analog card (KPCI-3130) to capture ringdown traces and provide control signals to various parts of the experiment [16]. At each wavelength in the spectrum, the optical cavity length is modulated slightly more than one free spectral range while monitoring transmitted light intensity. When sufficient buildup is observed, an acousto-optic modulator is de-energized thus shutting off the light into the cavity. The light intensity ringdown is then captured and stored. For each spectral step 200 ringdowns are obtained. Each ringdown is fit to a single exponential decay to determine its decay constant. Finally, the average decay is plotted versus wavelength to produce a spectrum. For gas sampling, an oil-free diaphragm pump (Drivac H-60) is used to cycle air

Downloaded from SAE International by Frank Tittel, Wednesday, June 27, 2018

through the cavity. This pump is mounted on a foam isolation pad to reduce vibrations. The pressure inside the cavity is monitored with a Leybold capacitance manometer and gauge (Combivac CM 33).

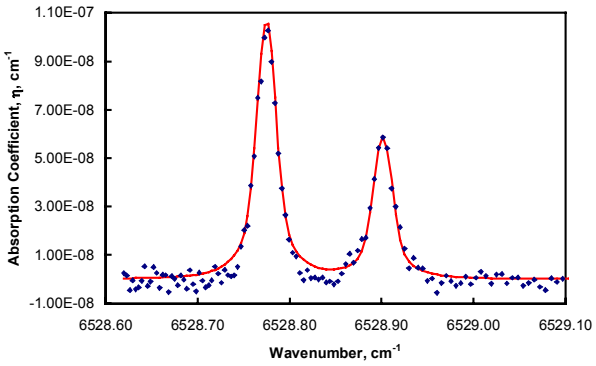

Figure 6: Ammonia spectrum using CRD spectrometer. Spectrum is of ammonia at 500 ppbV in a 67 Torr cell. Line drawn through data is a result of Voigt fitting routine.

Ammonia sensing with CRDS

Figure 6 shows a CRD spectrum of ammonia demonstrating high signal to noise ratio at sub ppmV levels. Ammonia was monitored in the laboratory air by monitoring the strongest line in the spectrum at 6528.8 cm^{-1}. Rather than collect an entire spectrum, points were taken at a skeletal set of wavelengths on and off resonance of the spectral feature for a total of 5 wavelengths. The time required to make each concentration determination was approximately 10 seconds. The sensor was programmed to acquire NH_3 concentration data every minute.

Figure 7 shows the results obtained for one day of sensor operation. Events labeled as “A” correspond to exposing the sensor to the vapor near an open bottle of concentrated ammonium hydroxide solution. Events labeled as “B” were samples of exhausted breath from various members of the laboratory staff indicating low (< 100 ppbV) levels of exhaled NH_3. At the point labeled as “C” in the time record the sampling valve was closed, but the sensor continued to run. The rising ammonia level is indicative of outgassing of ammonia from the walls of the CRD cell.

Analog Cavity Ringdown Analysis Circuit

In order to miniaturize the current cavity ringdown spectrometer, new electronics have been added to the system for improved performance and control. This upgrade includes an analog time constant measurement and more intelligent control of the piezoelectric driver for mirror positioning. A block diagram is shown schematically in Figure 8.

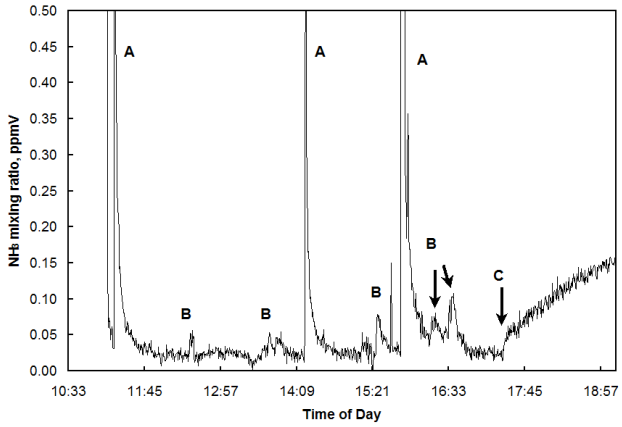

Figure 7: Ammonia sensing experiments using CRD spectrometer. (see text for details.)

An analog circuit receives the photodiode intensity signal and sequences the events occurring during data acquisition. The amplified photodiode signal must exceed a preset voltage threshold in order to trigger the circuitry. When this occurs, the laser is switched off using an acousto-optic modulator , the PZT voltage ramp is paused to hold the mirrors at the proper position for cavity resonance, and the ringdown timer is reset to zero. As the photodiode signal falls back below the threshold level, the ringdown timer is activated and begins producing a linear voltage ramp. When the signal has further decayed to one third of the threshold value, the ringdown timer is paused, and it holds the final voltage reached by the ramp. An analog to digital conversion of this final voltage then takes place and the signal is recorded with a commercial data acquisition system. The sequence is completed when the laser is switched on again. If the cavity is still in resonance, another ringdown event is recorded immediately. Otherwise, the PZT driver resumes its voltage ramp.

This circuit improves the function of the system in three important ways. First, significantly reduced requirements are placed on the analog to digital conversion process because only a single value must be generated per ringdown, and the conversion time may be significantly longer than the cavity ringdown time. This also reduces the computing power needed for signal processing as no curve-fitting algorithm is employed. Second, the cavity mirrors are held in position during the ringdown, so the cavity remains resonant during this time. Third, should the cavity remain resonant when the laser is switched on again, a

Downloaded from SAE International by Frank Tittel, Wednesday, June 27, 2018

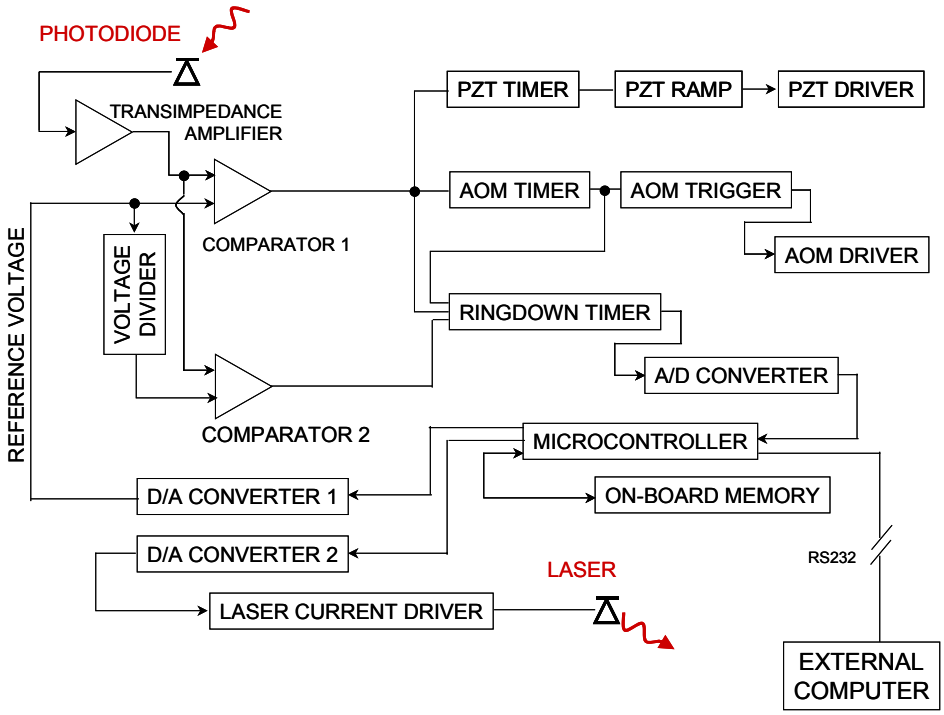

Figure 8: Functional schematic of analog cavity ring down electronics.

subsequent ringdown is immediately produced without the need to ramp the mirrors through another cycle. This results in greater experimental bandwidth.

TYPE II INTERBAND CASCADE LASER DEVELOPMENT

The availability of compact and efficient mid-infrared sources would dramatically enhance chemical sensing capabilities, since many gases of interest to NASA exhibit their fundamental (strongest) absorption lines in this wavelength range. Recently, the development of type-II interband cascade (IC) lasers [17, 18] for such an application has been advanced significantly at JPL [19-21] Here, we report some of our efforts in the development of single-mode distributed feedback (DFB) IC lasers.

For applications in chemical sensing, it is desirable for lasers to have a stable single-mode emission with tunability over a few wavenumbers. By incorporating a DFB grating into an IC laser structure, stable single-mode emission can be achieved. In this work, laser samples were grown in a molecular beam epitaxy (MBE) system on a nominally undoped *p*-type GaSb (001) substrate. A piece of the sample was first fabricated into Febry-Perot (FP) mesa stripe lasers (without DFB grating) to examine the appropriate wavelength

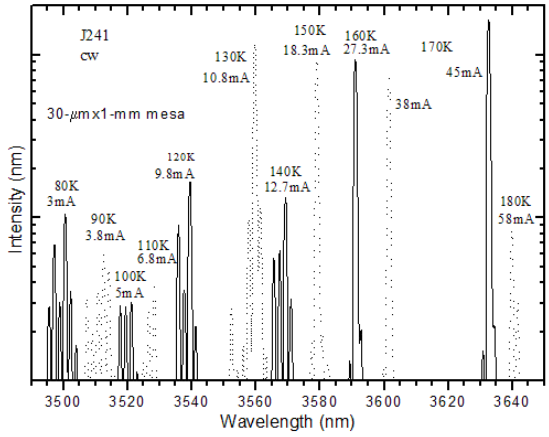

Figure 9: *cw* emission spectra of a FP laser operated in temperature range from 80 to 180K.

coverage with suitable device performance. A 30-μm-wide and 1-mm-long FP laser made from this sample operated in cw mode at temperatures up to 180 K covering wavelength range from ~3.5 to 3.64 μm (Figure 9), which indicates the suitability of the laser sample for being fabricated into a DFB laser with single mode emission near 3.53 μm for detection of H_2CO.

Downloaded from SAE International by Frank Tittel, Wednesday, June 27, 2018

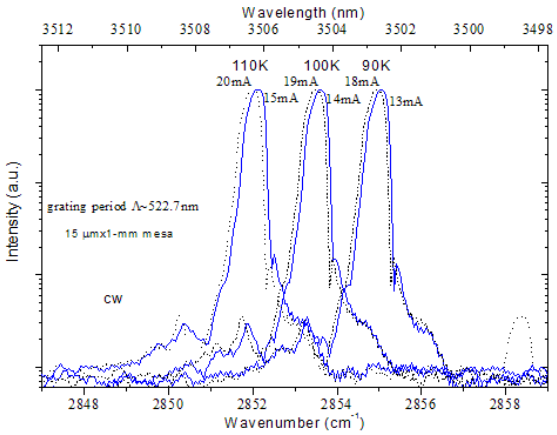

Figure 10: Spectra of a DFB laser at several current settings and at 90, 100, 110 K.

For DFB lasers, first-order gratings were formed on top of the laser sample by electron beam lithography and reactive ion etching. The sample was processed into 15-μm-wide and 1-mm-long mesa stripes with metal contact covering the top surface of the DFB grating. These lasers operated in cw mode in the temperature range from ~80 to ~185 K with emission wavelengths from ~3.5 to 3.6 μm. Figure 10 shows the lasing spectra of a DFB laser in the temperature range from 90 to 110 K with a stable single mode emission. Figure 11 summarizes the lasing wavelengths of four devices made from this sample with different grating periods (Λ~522.7, 523.8, 527.3, 530.9 nm), showing wavelength tuning as a function of temperature. DFB modes have a tuning rate of ~0.2 nm/K as governed mainly by temperature-dependent effective index n_{eff}. The wavelength of a DFB mode is essentially determined by the grating period Λ according to $\lambda=2n_{eff}\Lambda$, which is manifested by four DFB laser tuning curves with different grating periods as shown in Figure 11. FP modes were also observed from lasers made from this sample. The temperature dependence of a FP mode basically followed the variation of the band-gap (or material gain peak) with temperature and has a tuning rate of ~0.8 nm/K in the temperature range that we have examined. The obtained output powers of these lasers could be as high as 10 mW/facet at low temperatures (80-120 K) with low current injection (<60 mA) and still higher than a few miliwatts at relative high temperatures (120-170 K).

CONCLUSIONS AND FUTURE WORK

We have demonstrated that both QEPAS and cw-CRDS can be used to monitor ammonia at levels relevant to NASA's needs using readily available near infrared diode lasers. By extending the measurements into the mid infrared, detection limits will be lowered for both techniques and several new target molecules can be detected. Type II interband cascade lasers operating near 2850 cm^{-1} have been shipped to George Washington and Rice Universities. Using these lasers, the spectroscopy groups have demonstrated the detection of formaldehyde, which has a rich spectrum in this frequency region. Although several interfering water absorption features are also present here, spectroscopists have used isolated HCHO features to detect formaldehyde in the ambient atmosphere in the part per trillion level. Simulations suggest that a 10 ppbV level for formaldehyde will produce spectral features with α in excess of 10^{-8} cm^{-1}, a value above the detection limit for our instruments.

Acknowledgements

This work was supported by NASA grants with Darrell Jan serving as Technical Monitor.

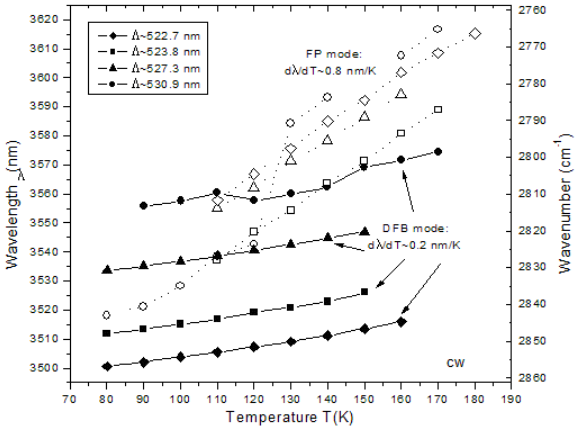

Figure 11: Wavelength tuning as a function of temperature that illustrates the difference in the tuning rate between a DFB (solid) and a Fabry-Perot (dotted) modes.

Downloaded from SAE International by Frank Tittel, Wednesday, June 27, 2018

References

1. Webber, M.E., D.S. Baer, and R.K. Hanson, *Ammonia monitoring near 1.5 mm with diode-laser absorption sensors.* Appl. Optics, 2001. **40**: p. 2031-2042.
2. Miklós, A., P. Hess, and Z. Bozóki, Application of acoustic resonators in photoacoustic trace gas analysis and metrology. Rev. Sci. Instr., 2001. **72**: p. 1937-1955.
3. Kosterev, A.A., et al., *Quartz-enhanced photoacoustic spectroscopy.* Optics Letters, 2002. **27**: p. 1902-1904.
4. Schmohl, A., M. A, and P. Hess, *Detection of ammonia by photoacoustic spectroscopy with semiconductors.* Appl. Optics, 2002. **41**(9): p. 1815-1823.
5. Weidmann, D., A.A. Kosterev, and F.K. Tittel, Application of a widely electrically tunable diode laser to chemical gas sensing with quartz-enhanced photoacoustic spectroscopy. Optics Letters, 2004. **submitted**.
6. Grober, R.D., et al., *Fundamental limits to force detection using quartz tuning forks.* Review of Scientific Instruments, 2000. **71**(2776).
7. Webber, M.E., M.Pusharsky, and C.K.N. Patel, Fiber-amplifier enhanced photoacoustic spectroscopy using near-infrared tunable duiode lasers,. 2003. **42**(12).
8. Pushkarsky, M.B., M.E. Webber, and C.K.N. Patel, Ultra-sensitive ambient ammonia detection using CO2-laser-based photoacoustic spectroscopy. Appl. Phys. B, 2003. **77**: p. 381-385.
9. O'Keefe, A., Chem. Phys. Lett., 1998. **293**: p. 331.
10. O'Keefe, A., J.J. Scherer, and J.B. Paul, Chem. Phys. Lett., 1999. **307**: p. 343-349.
11. Xie, J., et al., Chem. Phys. Lett., 1998. **284**: p. 387-395.
12. Scherer, J.J. and D.J. Rakestraw, Chem. Phys., 1995. **102**: p. 5269.
13. Scherer, J.J., et al., Chem. Rev., 1997. **97**: p. 25-51.
14. Paldas, B.A., et al., J. of Appl. Phys., 1998. **83**(8): p. 3991-3997.
15. Provencal, R.A., et al., Spectroscopy, 1999. **14**(4): p. 24-33.
16. Awtry, A. and J.H. Miller, Development of a cw-laser-based cavity-ringdown sensor aboard a spacecraft for trace air constituents. Applied Physics B, 2002. **75**: p. 255-260.
17. Yang, R.Q., Superlattices and Microstructures, 1995. **17**: p. 77.
18. Yang, R.Q. *Microstructures and Microdevices*. in *7th Inter. Conf. on Superlattices*. 1994. Banff, Canada: Superlattices and Microstructures.
19. Yang, R.Q., et al., Appl. Phys. Lett., 2003. **15**: p. 2109.
20. Hill, C.J., B. Yang, and R.Q. Yang, Physica E, 2004. **20**: p. 486.
21. R. Q. Yang, et al., Appl. Phys. Lett., 2004. **in press**.